sustainability

Article

Research on Optimal Cooling Landscape Combination and Configuration Based on Local Climate Zones—Fuzhou, China

Yuanbin Cai [1,*,†], Chen Gao [1,†], Wenbin Pan [1], Yanhong Chen [2,3] and Zijing Wu [1]

1 College of Environment & Safety Engineering, Fuzhou University, Fuzhou 350108, China; 13290951273@163.com (C.G.); wenbinpan@fzu.edu.cn (W.P.); w18057520599@163.com (Z.W.)
2 Key Laboratory of Humid Subtropical Eco-Geographical Process of Ministry of Education, Fujian Normal University, Fuzhou 350007, China; cyh2008@sohu.com
3 Department of Environmental and Resources Engineering, Fuzhou University Zhicheng College, Fuzhou 350002, China
* Correspondence: caiyuanbin82@163.com; Tel.: +86-133-8591-4526
† These authors contributed to this work equally.

Abstract: The deterioration of the urban thermal environment has seriously affected the quality of life of urban residents, and studying the optimal cooling landscape combination and configuration based on local climate zones (LCZs) is crucial for mitigating the thermal environment. In this study, the LCZ system was combined to analyze the spatial and temporal changes to the thermal environment in the central area of Fuzhou, and the 159 blocks in the core area were selected to derive the optimal LCZ combination and configuration. The conclusions are as follows: (1) From 2013 to 2021, the building layout of the study area became more open and the building height gradually increased. The high-temperature areas were mainly clustered in the core area; (2) The LSTs for low-rise buildings (LCZ 3 (41.67 °C), LCZ 7 (40.10 °C), LCZ 8 (42.61 °C), and LCZ 10 (41.85 °C)) were higher than the LSTs for high-rise buildings (LCZ 1 (38.58 °C) and LCZ 4 (38.50 °C)); (3) The thermal contribution index for low building types was higher for dense buildings (LCZ 3 (0.4331), LCZ 8 (0.3149), and LCZ 10 (0.2325)) than for open buildings (LCZ 6 (0.0247) and LCZ 9 (0.0317)); (4) Blocks with an average LST of 36 °C had the most cost-effective cooling, and the combination and configuration of LCZs within such blocks were optimal. Our results can be used to better guide urban planners in managing LCZ combinations and configurations within blocks (the smallest planning unit) at an earlier phase of thermal environment design, and for appropriately adapting existing block layouts, providing a new perspective on urban thermal environment research with important implications for climate-friendly city and neighborhood planning.

Keywords: local climate zones; land surface temperature; thermal contribution; landscape composition; landscape configuration

check for updates

Citation: Cai, Y.; Gao, C.; Pan, W.; Chen, Y.; Wu, Z. Research on Optimal Cooling Landscape Combination and Configuration Based on Local Climate Zones—Fuzhou, China. *Sustainability* **2024**, *16*, 2367. https://doi.org/10.3390/su16062367

Academic Editor: Joern Birkmann

Received: 8 February 2024
Revised: 26 February 2024
Accepted: 9 March 2024
Published: 13 March 2024

1. Introduction

Against the dual background of global warming [1] and rapid urbanization, the gradual deterioration of the urban thermal environment has become a prominent feature of the modern urban climate [2–4]. The urban heat island (UHI) effect, which is defined as a temperature phenomenon caused by rapid urbanization and industrialization, is the concentrated response and manifestation of the deterioration of the urban thermal environment whereby temperatures in urban areas are higher than those in the surrounding rural areas, creating a phenomenon similar to a heat island [5,6]. Rapid urbanization has directly led to reductions in urban subsurface albedo, vegetation cover, and evapotranspiration, as well as a significant increase in anthropogenic waste heat emissions, which are key factors in the formation of the UHI [7–10].

The land surface temperature (LST) is a central parameter in the study of the urban thermal environment [7]. The land cover type of the urban surface is significantly correlated with the LST [11,12]. Previous studies have shown that increases in blue-green spaces such as vegetation and water bodies can reduce the LST [13,14], while increases in impervious surfaces such as built-up land and bare ground can increase the LST [12,15]. However, the area of blue-green space left in the city is very limited, so it is difficult to cool down by directly increasing it. Many studies have examined the relationship between the spatial configuration of land cover patches and the LST, and the results suggest that the LST can be reduced by optimizing the spatial configuration of land cover types to mitigate UHIs [16–18]. Arijit Das studied the impact of the spatial composition and structure of the impervious surface (IS), green space (GS), and blue space (BS) on the thermal environment from multiple geospatial and statistical perspectives [19]. Jinyao Lin used morphological spatial pattern analysis to spatially visualize various land use elements from the perspective of mathematical morphology, explored the influence of the spatial pattern of built-up areas on urban surface heat islands, and determined the correlation between the intensity of SUHIs in the study area and the proportions of the core, fringe, bridge, and small islands of the built-up area [20]. These studies do not consider additional landscape indices, landscape types, and spatial metrics at the landscape level, and urban planning still lacks a comprehensive integration of urban climate elements. Despite many studies exploring the relationship between the urban heat island effect and landscape assemblages and configurations, a range of landscape metrics and spatial patterns of temperature change cannot be integrated with urban planning factors, leading to difficulties in practically guiding the planning of thermally adapted cities [21,22].

The effective implementation of UHI mitigation strategies remains challenging due to professional barriers between the planning and meteorological disciplines and the lack of comprehensive integration of urban climate elements in urban planning [18,23]. There are no criteria for the selection of study sites, and the combination and configuration of land cover types cannot be analogized between different cities, which has prevented researchers from providing a scientific and in-depth explanation of the relationship between urban planning and design factors and temperature [24,25]. The Local Climate Zone (LCZ) system effectively distinguishes the thermal characteristics of different urban buildings based on their surface structures, materials, and land cover types [5,26]. Clear definitions and classification criteria for each LCZ type can be applied to analyze and compare urban heat islands worldwide [27]. The LCZ system can further quantify the link between the urban fabric and the thermal environment, providing an effective way to break down the language barrier between urban climate and urban planning [24,28,29]. More than 130 cities worldwide have studied the classification of UHIs based on the LCZ system [30]. The LCZ system has become a common classification system and research method for urban thermal environment researchers and urban planners [31].

However, the LCZ is underused as a standardized system for breaking down the barriers of urban planning and urban climate language [21,32,33], and studies examining the composition and configuration of landscapes based on LCZ systems have received less attention. Optimal cooling LCZ compositions and configurations have not been explored, which limits the ability to make concrete recommendations for actionable planning and management [27,34].

This study analyzes the spatial and temporal changes in the thermal environment in the central urban area of Fuzhou from 2013 to 2021 based on the LCZ classification. The road network is used to divide the study area into different subdistrict blocks, and 159 blocks in the core area are selected to further explore the optimal LCZ combinations and configurations. We discuss and analyze the following issues: (1) the spatial and temporal changes of LCZs and the thermal environment in the central city of Fuzhou from 2013 to 2021; (2) the cooling/warming effects of LCZ combination types; (3) the thermal contributions of LCZ types; (4) ways in which the combination and configuration of LCZ types in a neighborhood affect heating and cooling; and (5) optimal LCZ combinations and configurations. This study proposes for the first time the most cost-effective LCZ combinations and configurations for cooling in the core area blocks of Fuzhou's central city, which can be used as a reference for adjusting the spatial layout of high surface temperature zones in the study area and practically alleviate the city's heat island effect from the urban planning point of view.

2. Materials and Methods

2.1. Study Area

Fuzhou is the capital of Fujian province, located in China's eastern coastal region. It is an important hub city connecting the inland with ASEAN and Taiwan, and an ecologically livable riverside and coastal international metropolis (Figure 1a). Fuzhou is located within an estuary basin surrounded by mountainous terrain with an elevation of 600–1000 m (Figure 1b) [35]. With the rapid development of urbanization, Fuzhou has experienced great changes in the urban surface and a significant urban heat island effect, becoming the new "furnace city" in China [36]. In 2020, the number of high-temperature (>35 °C) days in Fuzhou reached 87, and the number of extreme high-temperature (>40 °C) days reached 3 [37]. While the central city has the most strategic position in the overall pattern of land space in Fuzhou, it faces serious thermal environment problems [38]; therefore, mitigating the thermal environment by studying the optimal cooling landscape combinations and configurations is worth investigating. Therefore, we refer to the central urban area in the Fuzhou land and space master plan (2021–2035) as the study area, which covers an area of about 2001 km^2 (Figure 1c).

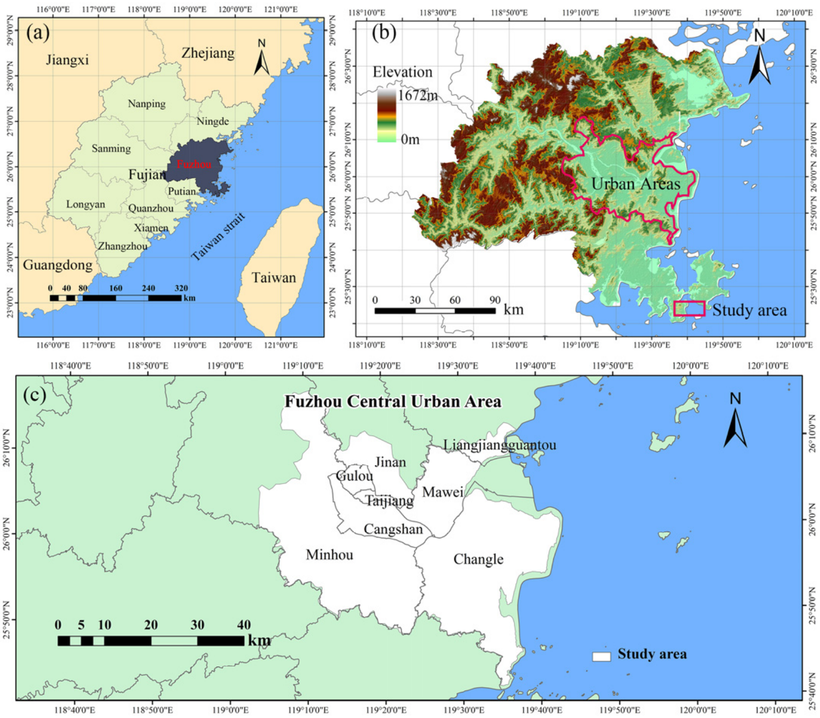

Figure 1. Location of the Fuzhou central urban area. (**a**) Location of Fuzhou in Fujian province; (**b**) The elevation of Fuzhou and the boundary of the study area; and (**c**) Location of the Fuzhou central urban area.

2.2. Data

We used the Landsat series of satellite remote sensing data downloaded from the websites of the Chinese Academy of Sciences (https://www.gscloud.cn accessed on 1 October 2022). The selected image orbital number is 119/42, the cloud cover was less than 5%, and the imaging time was summer (June~September) in Fuzhou city. Due to the weather limitations, such as cloud cover and atmospheric pollution, 3 images were selected to characterize the dynamics of LST and LCZ (Table 1).

Table 1. Remote sensing data.

Time	Sensor	Cloud Cover (%)	Usage
4 August 2013 27 July 2016 27 September 2021	Landsat-8 OLI; Landsat-8 TIRS	<5	LCZ classification and LST retrieval

In addition, high-resolution historical Google images and open street maps (https://www.openstreetmap.org/, accessed on 21 June 2023) were used as auxiliary tools to extract training samples to obtain LCZ classification maps and divide blocks. Fuzhou land and space master plan (2021–2035) (http://www.fuzhou.gov.cn/, accessed on 10 June 2023) were used to determine the vector boundaries of Fuzhou's central urban area. Fuzhou city meteorological data (http://data.cma.cn/, accessed on 15 October 2022) were used to validate the accuracy of the surface temperature inversion data.

2.3. Methods

2.3.1. LCZ Classification

LCZs refer to a classification system with 17 classes, including 10 building LCZ 1-10 sub-standard classes and 7 land cover LCZ A g sub-standard classes (Table 2) [24]. The LCZ classification map is mainly used for a city or a specific research area, employing satellite imagery [39–41] or GIS data [42–44] to generate a map to visualize the surface morphology and local climate of the city. According to the different data sources and analysis methods, there are three main methods of LCZ classification: manual sampling, remote sensing, and vectors in the GIS environment [43]. Most previous studies have used raster-based open source data and software such as the World Urban Database and Access Portal Tools (WUDAPT, https://www.wudapt.org/, accessed on 10 June 2023) to map LCZs [25,33,45–48]. Remote sensing provides a rapid and low-cost method of LCZ classification using open source remote sensing images. To support this method, the WUDAPT was developed to generate LCZ maps by analyzing satellite images with semi-automated image classification algorithms [28,49,50]. In this study, an LCZ classification map was constructed for the Fuzhou central urban area using WUDAPT [33], and following five steps:

(1) Based on the region of interest (ROI), Landsat-8 images of Fuzhou's central urban area from 2013, 2016, and 2021 that met the criteria of having less than 5% cloud cover and being daytime images (i.e., 4 August 2013, 27 July 2016, 27 September 2021) were downloaded from the websites of the Chinese Academy of Sciences (https://www.gscloud.cn, accessed on 1 October 2022).
(2) These satellite images were preprocessed and resampled to 100 m from the original 30 m to represent the spectral signal of the local-scale urban structure instead of that of smaller objects.
(3) The WUDAPT guidelines were followed to select training areas via Google Earth (Table 2). More than ten training areas for each type of LCZ were digitized and evenly distributed across the study area.
(4) Based on the Landsat-8 images and the training samples, an LCZ map of the study area was generated using a random forest (RF) method in SAGA-GIS.
(5) A set of assessment points was generated to evaluate the accuracy of the LCZ mapping results using overall accuracy (OA). To assess the accuracy of the LCZ classification, the predicted and observed LCZ types for the selected points were compared and evaluated using the error matrix or the so-called confusion matrix.

Table 2. LCZ types and corresponding training samples in the Fuzhou central urban area.

LCZ 1 (compact high-rise)	LCZ 2 (compact mid-rise)	LCZ 3 (compact low-rise)
 	 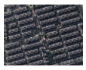	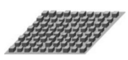 
LCZ 4 (open high-rise)	LCZ 5 (open mid-rise)	LCZ 6 (open low-rise)
 	 	 
LCZ 7 (lightweight low-rise)	LCZ 8 (large low-rise)	LCZ 9 (sparsely built)
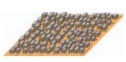 	 	 
LCZ 10 (heavy industry)	LCZ A (dense trees)	LCZ B (scattered trees)
 	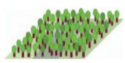 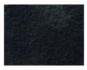	 
LCZ C (bush scrub)	LCZ D (low plants)	LCZ E (bare rock or paved)
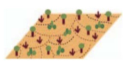 	 	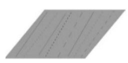 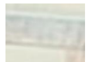
LCZ F (bare soil or sand)	LCZ G (water)	
 	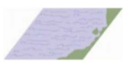 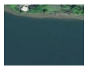	

2.3.2. LST Retrieval

Because of the diverse sources, the remote sensing data used to obtain the surface temperature information inversion principle have certain differences [51]. At present, domestic and foreign researchers propose a variety of inversion of surface temperature algorithms according to the characteristics of different thermal infrared remote sensing data [52,53]. These algorithms can be broadly categorized into three types: the single-channel algorithm, multi-channel algorithm, and splitting window algorithm (split window algorithm) [54]. The single-channel algorithm includes the radiative conduction equation method (atmospheric correction method) [53].

In this paper, the radiative conduction equation method was used to perform surface temperature inversion on the preprocessed Landsat-8 image.

2.3.3. Calculation of Contribution Metrics

Due to the fact that remote sensing images are acquired at different times, there may be differences in temperature between months. Therefore, the contribution index (CI) was used to compare the contribution degree of the thermal environment in different regions of each LCZ in different years [55,56]. The calculation formula is as follows:

$$CI = (\overline{LST_i} - \overline{LST}) \times \frac{S_i}{S} \tag{1}$$

where CI is the contribution index of the regions; i denotes the specific region; $\overline{LST_i}$ is the average temperature of the ith region; $\overline{LST}$ is the average surface temperature of the study area; S_i is the area of the ith region; and S is the total area of the study area. $CI > 0$ indicates that the ith region contributes positively to the increase in surface temperature. Conversely, $CI < 0$ indicates that area i contributes negatively to the increase in surface temperature.

2.3.4. Correlation Analysis of LCZ and LST

Regression models can help us evaluate the relationship between two or more attributes of a feature and are widely used to study the influencing factors of LSTs [22,57]. The ordinary least squares regression (OLS) and Spatial Lag Model (SEM) were used to investigate the relationship between LSTs at the parcel level and the distribution of LCZ combinations [58].

The OLS model is a common method for the statistical analysis of the interdependence between dependent variables and explanatory variables and is a statistical regression model with non-spatial attributes based on the assumption that each point of the dependent variable is spatially independent [59]. It is calculated as follows:

$$y_i = \sum_k \beta_k x_{ik} + \beta_0 + \varepsilon_i \tag{2}$$

where i represents the value of the sample-dependent variable at the ith point of the green patch in each period; k denotes an explanatory variable with significant correlations; β_k denotes the quantitative coefficient of the k-th explanatory variable; β_0 represents a constant term coefficient; ε_i denotes the residuals of the sample.

The SLM model expresses the meaning of a variable in a research unit in space, which has a feedback effect on the same variable in other research units in the surrounding spatial location. It is calculated as follows:

$$Y = \rho WY + X\beta + \varepsilon \tag{3}$$

where Y represents an n $\times$ 1 vector as the dependent variable; n is the total number of green patch samples in each period; ρ represents the spatial correlation coefficient; W is the dependent variable spatial weight matrix of dimensions n $\times$ n; X is the n $\times$ k matrix of independent variables; β is the explanatory variable coefficient of dimensions $k \times 1$; and β represents the residuals of the sample.

3. Results

3.1. *Characteristics of Spatial and Temporal Variations in LCZ Classification*

Based on the LCZ classification process, we obtained the distribution of the 2013, 2016, and 2021 LCZs in Fuzhou's central urban area, as illustrated in Figure 2. The overall accuracy of the LCZ classification for each year was 76.18% (Table S1), 64.50% (Table S2), and 66.20% (Table S3), respectively.

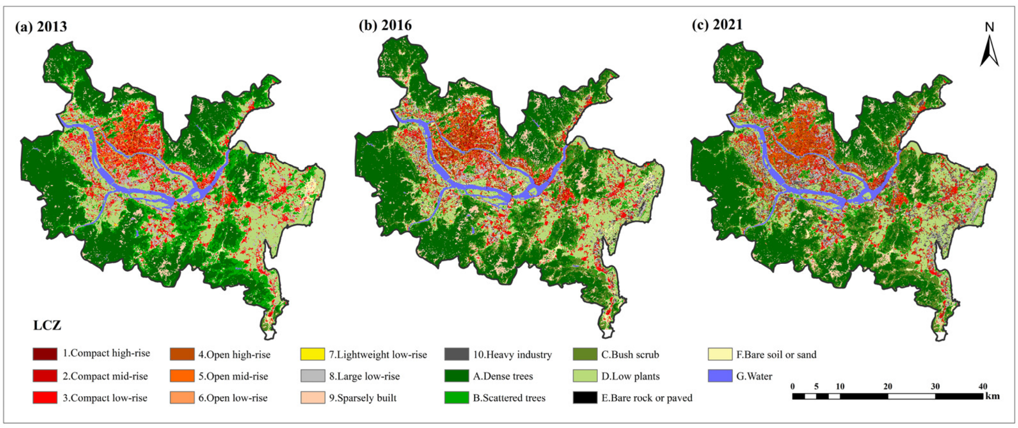

Figure 2. LCZ classification map in the study area.

Combining the changes in the area of LCZ types (Table 3), it can be seen that the LCZs in the study area changed significantly during the 8-year period. Among them, the area of LCZ 4 increased by 131.96 km^2, the most drastic change in number, with annual growth rates of 304.15%, 9.24%, and 172.54% in 2013–2016, 2016–2021, and 2013–2021, respectively. In terms of building height, the areas of low-rise buildings such as LCZ 3, LCZ 6, LCZ 7, and LCZ 8 all decreased, with decreases of 58.68, 3.65, 6.85, and 5.05 km^2, whereas the areas of medium- and high-rise buildings such as LCZ 1, LCZ 2, LCZ 4, and LCZ 5 increased, with increases of 7.18, 8.96, 131.96, and 29.43 km^2. Mid- and high-rise buildings replaced some of the low-rise buildings as the predominant building type, indicating a gradual increase in average building heights in the study area. In terms of building density, the areas of dense buildings such as LCZ 1, LCZ 2, and LCZ 3 decreased by a total of 42.54 km^2, while the areas of open buildings such as LCZ 4, LCZ 5, and LCZ 6 increased by a total of 157.74 km^2, with open buildings replacing some of the dense buildings, which indicates that the layout of the buildings in the study area became more open.

Table 3. Changes in LCZ area in the study area from 2013 to 2021.

LCZ Type		Area (km^2)			Change Area (km^2)	Annual Rate of Change (%)		
		2013	2016	2021	2013–2021	2013–2016	2016–2021	2013–2021
Built Types	1	11.66	14.65	18.84	7.18	8.55	5.72	7.70
	2	119.54	124.93	128.50	8.96	1.50	0.57	0.94
	3	139.34	112.78	80.66	−58.68	−6.35	−5.70	−5.26
	4	9.56	96.79	141.52	131.96	304.15	9.24	172.54
	5	25.35	47.70	54.78	29.43	29.39	2.97	14.51
	6	21.91	17.04	18.26	−3.65	−7.41	1.43	−2.08
	7	10.40	2.03	3.55	−6.85	−26.83	14.98	−8.23
	8	25.02	14.61	19.97	−5.05	−13.87	7.34	−2.52
	9	76.28	35.76	31.89	−44.39	−17.71	−2.16	−7.27
	10	12.04	31.09	59.34	47.30	52.74	18.17	49.11
Land Use Types	A	744.4	714.88	699.04	−45.36	−1.32	−0.44	−0.76
	B	145.27	110.31	112.38	−32.89	−8.02	0.38	−2.83
	C	163.60	173.29	204.84	41.24	1.97	3.64	3.15
	D	371.28	338.37	324.80	−46.48	−2.95	−0.80	−1.56
	E	7.52	12.91	6.15	−1.37	23.89	−10.47	−2.28
	F	34.65	71.67	20.14	−14.51	35.61	−14.38	−5.23
	G	80.48	80.88	75.05	−5.43	0.17	−1.44	−0.84

Among the land cover types, only LCZ C increased in area by 41.24 km^2, while the others decreased. Among them, LCZ A and LCZ D had the highest area percentages in the study area and the highest reduction in area, with 45.36 and 46.48 km^2, respectively, which indicated that the increase in bush scrub was accompanied by a significant abatement of dense trees. The overall decreases in LCZ E, LCZ F, and LCZ G were 1.37, 14.51, and 5.43 km^2, respectively, with annual decreases of 2.28%, 5.23%, and 0.84%, respectively, without much change.

3.2. Spatial–Temporal Variation Analysis of Temperature Based on LCZ Classification

We used weather station data to validate the LST retrieval results. The errors between the atmospheric temperatures and the inversion temperatures in this study are all within the acceptable range of 1 °C [60,61] (Table S4), so the temperatures obtained by the inversion can be used to characterize the surface temperatures. By combining Figure 3 and Table 4, it can be seen that the average and maximum surface temperatures in the central area of Fuzhou showed a fluctuating trend of first increasing and then decreasing from 2013 to 2021. In addition, high-temperature zones were mainly clustered in the Fuzhou core area (within the third ring of the road network). This area mainly consists of commercial areas, industrial areas, residential areas, and pending construction sites with intensive population activity.

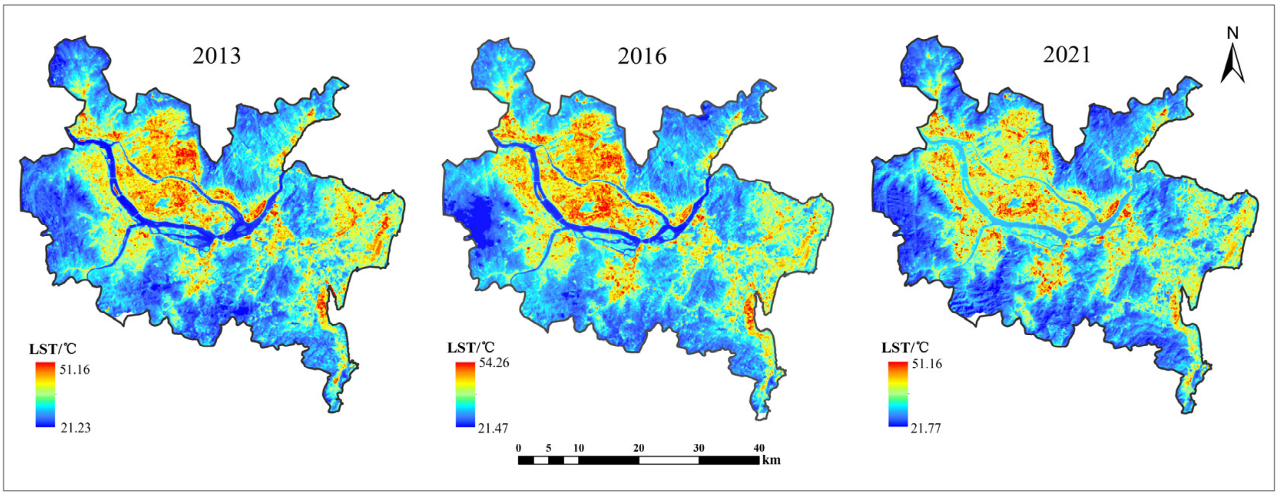

Figure 3. Changes in LCZ area in the study area from 2013 to 2021.

Table 4. LST statistics result.

Year	LST (°C)			
	Mean	**Minimum**	**Maximum**	**Standard Deviation**
2013	32.30	21.23	51.16	4.638
2016	36.54	21.47	54.26	4.367
2021	31.26	21.77	51.16	3.986

To investigate the thermal environment characteristics of LCZ types, LSTs and box plots of LCZ categories were obtained by means of the superposition analysis method (Figure 4, Table 5). The results indicate that the LST distribution in the study area correlated with the LCZ distribution [62]. In terms of LST differences among LCZ types, the highest mean LSTs were found in low-rise buildings (LCZ 3 (41.67 °C), LCZ 7 (40.10 °C), LCZ 8 (42.61 °C), and LCZ 10 (41.85 °C)), while the lowest mean LSTs were found in sparsely built areas (LCZ 9 (35.77 °C)), and lower mean LSTs were found in high-rise buildings (LCZ 1 (38.58 °C) and LCZ 4 (38.50 °C)). Among the land cover types, LCZ A (31.62 °C) and LCZ G (30.58 °C) had the lowest mean LSTs, LCZ E (41.18 °C) and LCZ F (38.34 °C) had the highest mean LSTs, and LCZ D also had a mean LST of 37.16 °C, which suggests that LCZ D also had a significant effect on the increase in the LST.

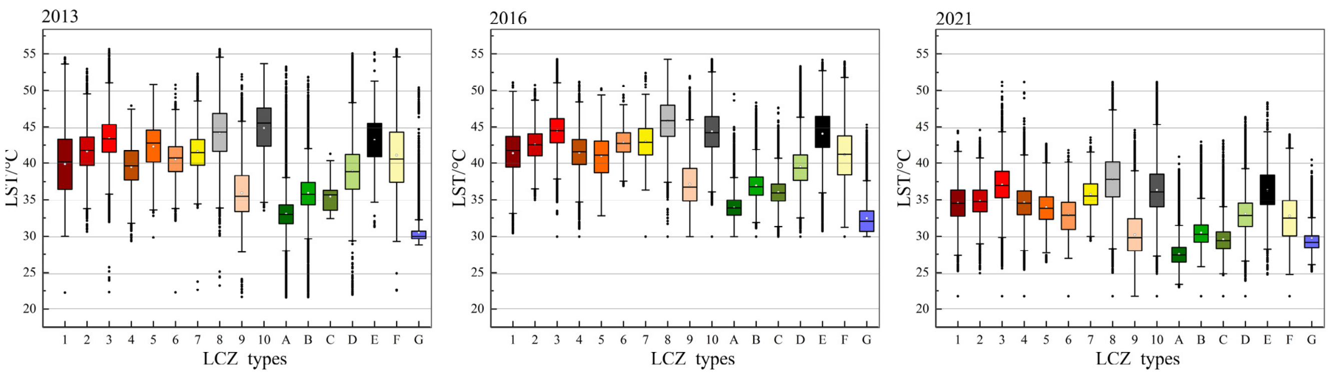

Figure 4. Box-plots of LST distributions in LCZ.

Table 5. LST statistics of LCZ types.

LCZ Build Types	LST (°C)				LCZ Land Cover Types	LST (°C)			
	2013	**2016**	**2021**	**Mean**		**2013**	**2016**	**2021**	**Mean**
1	39.87	41.35	34.52	38.58	A	33.05	33.90	27.91	31.62
2	41.62	42.57	34.85	39.68	B	35.92	35.17	30.51	33.87
3	43.44	44.48	37.10	41.67	C	35.44	35.49	29.57	33.50
4	39.47	41.43	34.60	38.50	D	38.94	39.50	33.05	37.16
5	42.31	40.99	33.95	39.08	E	43.17	44.07	36.31	41.18
6	40.52	42.84	32.89	38.75	F	41.10	41.17	32.74	38.34
7	41.60	42.96	35.74	40.10	G	30.53	32.46	28.75	30.58
8	44.16	45.83	37.85	42.61					
9	36.94	37.16	33.21	35.77					
10	44.84	44.38	36.33	41.85					

We further counted the LSTs of the LCZ combination types (Table 6), in which the low and denser LCZs (3, 8, 10) had the highest mean LST of 41.88 °C, in contrast to the low and open LCZs (6, 9), where the mean LST was only 34.61 °C, indicating that the effect of the dense building type on the mean LST was significantly larger than the effect of open building types on the mean LST [63]. The mean temperatures of LCZs (1~10) and LCZs (A~G) were 39.48 °C and 33.83 °C, respectively. When divided into natural and constructed land, the mean temperatures of LCZs (A~C, G) and LCZs (1~10, D~F) were 32.29 °C and 38.30 °C, respectively. In terms of building height, the highest mean temperatures were observed in 2013 and 2016 for the mid-rise building-type LCZs (2, 5). In 2021, the highest mean temperatures were observed for the low-rise building-type LCZs (3, 6, 8, 9). The mean temperature differences between the high, medium, and low building types varied between 0.5 and 2.3 °C in all periods.

Table 6. LST statistics of LCZ combinatorial types.

LCZ Combination	Type Description	LST/(°C)			
		2013	**2016**	**2021**	**Mean**
LCZs (1~10)	Built type	41.44	41.81	35.19	39.48
LCZs (A~G)	Land use type	35.45	36.26	29.78	33.83
LCZs (A~C, G)	Natural land	33.82	34.58	28.47	32.29
LCZs (1~10, D~F)	Constructed land	40.04	40.71	34.15	38.30
LCZs (3, 8, 10)	Low-profile dense built	43.70	44.83	37.10	41.88
LCZs (6, 9)	Low open built	36.27	37.21	30.35	34.61
LCZs (1, 4)	High-level built	39.68	41.42	34.60	38.57
LCZs (2, 5)	Medium-level built	41.87	41.93	34.56	39.45
LCZs (3, 6, 8, 9)	Low-level built	41.43	41.53	36.87	39.94

3.3. Quantification of the Cooling/Warming Effect of LCZ Combination Types

The conclusions in Section 3.2 suggest that LSTs in the central part of Fuzhou were related to LCZs. Based on the road network, the study area was divided into 550 blocks, and the average temperature as well as the areas of the LCZ types were considered together. The LCZs (3, 8, 10), LCZs (6, 9), LCZs (1~10), and LCZs (A~C, G) combination types that had a large influence on the LST change were selected, and the area shares of the four LCZ combination types in the 550 blocks were calculated and used as the independent variable factor. The fraction vegetation coverage (FVC), which was considered by previous authors to have the greatest influence on the LST [64], was also used as an independent variable factor. In this paper, OLS and SEM were used to quantify the cooling/warming effects of these five factors. The parameters compared between linear regression models and autoregressive models included p-value (probability), R^2, LIK (log-likelihood), AIC (Akaike information criterion), and SC (Schwarz criterion) [58,65]. The higher the R^2 value, the stronger the correlation. The larger the LIK and the smaller the AIC and SC, the better fitting and more credible the model.

It can be seen that both models have significance, and almost all influencing factors passed the significance test ($p < 0.05$) (Table 7). Both regression models explained over 80% of the total degree of variation where a positive coefficient value meant that the factor showed a positive correlation with the block temperature and a negative coefficient value meant a negative correlation with the temperature. The regression coefficients of LCZs (1 to 10) and LCZs (3, 8, and 10) were all positive, with a warming effect, and all other things being equal, an increase in the proportion of the area to the block will be followed by an increase in the temperature of the block, which confirms the conclusions of Section 3.2. The variable that explained the most about the LST was LCZ (1–10), and in the case of the OLS model for 2016 temperatures, for example, the coefficient of LCZs (1–10) was 7.7026, which implies that all else being equal, for every 1% increase in the proportion of the block area accounted for by LCZs (1–10), the temperature of the block will increase by 7.7026 °C. The regression coefficients of LCZs (6, 9), LCZs (A~C, G), and FVC were all negative with a cooling effect. In 2013 and 2021, LCZs (A~C, G) had the most significant moderating effect on the LST, and the regression coefficients were negative, indicating that an increase in the proportion of natural surface area within the zones reduced the temperature of the zones. Unlike in 2016, LCZs (6, 9) had the best explanatory effect on the LST, which was related to the fact that an increase in the area share of LCZs (6, 9) in blocks within the study area was usually accompanied by an increase in the area of blue-green space along with a decrease in the amount of dense built-up area.

Table 7. Comparison of model coefficients and fitting accuracy between OLS and SEM.

Time	Variable	Ordinary Least Square (OLS)		Spatial Lag Model (SEM)	
		Coefficient ± S.D.		Coefficient ± S.D.	
2013	LCZs (3, 8, 10)	1.0826 ± 0.6445	R^2 = 0.846575 LIK = 1109.17 AIC = −2230.34 SC = −2256.2	1.19678 ± 0.6282	R^2 = 0.852669 LIK = 1098.34 AIC = −2210.68 SC = −2240.85
	LCZs (6, 9)	−3.4560 ± 1.4808		−3.07154 ± 1.4452 *	
	LCZs (1~10)	7.3113 ± 0.5726 ***		7.16292 ± 0.5583 ***	
	LCZs (A~C, G)	−4.9943 ± 0.3563 ***		−4.62817 ± 0.3542 ***	
	FVC	−0.5123 ± 0.5256		0.0952 ± 0.5158	
2016	LCZs (3, 8, 10)	2.9301 ± 0.5930 ***	R^2 = 0.827147 LIK = 1167.12 AIC = −2346.24 SC = −2372.1	2.9887 ± 0.5673 ***	R^2 = 0.841941 LIK = 1145.74 AIC = −2305.48 SC = −2335.65
	LCZs (6, 9)	−7.8524 ± 1.3889 ***		−6.6620 ± 1.3347 ***	
	LCZs (1~10)	7.7026 ± 0.4714 ***		7.41245 ± 0.4505 ***	
	LCZs (A~C, G)	−7.1459 ± 0.4242 ***		−6.38758 ± 0.4173 ***	
	FVC	3.4212 ± 0.5682 ***		3.5554 ± 6.5429 ***	
2021	LCZs (3, 8, 10)	3.6538 ± 0.3509 ***	R^2 = 0.865119 LIK = 921.257 AIC = −1854.51 SC = −1880.37	3.7096 ± 0.3433 ***	R^2 = 0.869532 LIK = 912.301 AIC = −1838.6 SC = −1868.77
	LCZs (6, 9)	−2.4903 ± 0.9520 ***		−1.9166 ± 0.9392 *	
	LCZs (1~10)	3.1150 ± 0.2915 ***		3.0187 ± 0.2851 ***	
	LCZs (A~C, G)	−3.2762 ± 0.2989 ***		−3.0376 ± 0.2983 ***	
	FVC	−2.0851 ± 0.4091 ***		−1.8922 ± 0.4020 ***	

*** Significant at the 0.001 level. * Significant at the 0.05 level.

3.4. LCZ Types CI to Temperature

The CI was used to quantify the degree of warming or cooling for each LCZ type, and the CI values for the 10 building types in the study area from 2013 to 2021 were all positive (Figure 5, Table 8), indicating a positive contribution to the temperature of the study area. Among them, LCZ 3 (0.4331), LCZ 8 (0.3149), and LCZ 10 (0.2325) had the largest thermal contributions, which suggests that the low and denser LCZs (3, 8, 10) were the main contributors to the LST increase [63]. In contrast, LCZ 6 (0.0247) and LCZ 9 (0.0317) had smaller thermal contributions, suggesting that the low and open LCZs (6, 9) contributed relatively less to the LST increase. This indicates that the thermal contribution of dense building types is significantly higher than that of open building types in low-rise building types [66], which is in line with the conclusion in Section 3.2.

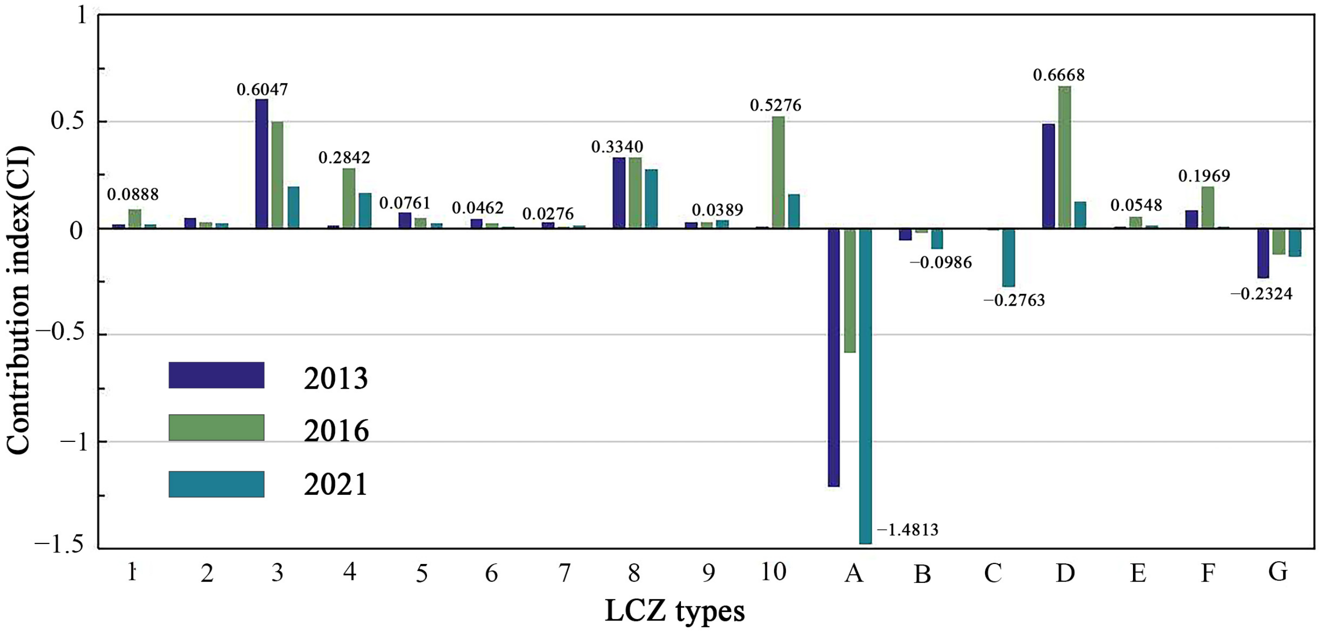

Figure 5. The CI of different LCZ types to temperature in the study area from 2013 to 2021.

Table 8. The CI of different LCZ types in the study area.

LCZ Build Types	CI				LCZ Land Cover Types	CI			
	2013	2016	2021	Mean		2013	2016	2021	Mean
1	0.0208	0.0888	0.0213	0.0436	A	−1.2121	−0.5823	−1.4813	−1.0919
2	0.052	0.0313	0.0239	0.0357	B	−0.0589	−0.0201	−0.0986	−0.0592
3	0.6047	0.4997	0.195	0.4331	C	−0.0001	−0.0043	−0.2763	−0.0936
4	0.0151	0.2842	0.1656	0.1550	D	0.4908	0.6668	0.1278	0.4285
5	0.0761	0.0482	0.0218	0.0487	E	0.0087	0.0548	0.0124	0.0253
6	0.0462	0.0256	0.0023	0.0247	F	0.0831	0.1969	0.0048	0.0949
7	0.0276	0.0075	0.0062	0.0138	G	−0.2324	−0.1242	−0.132	−0.1629
8	0.334	0.3317	0.2791	0.3149					
9	0.0274	0.0289	0.0389	0.0317					
10	0.0087	0.5276	0.1613	0.2325					

Among the land cover types, LCZ A, LCZ B, LCZ C, and LCZ G had negative CI values, indicating a negative contribution to the temperature in the study area, and were the major land cover types in slowing down the rise in the LST [66]. Among them, LCZ A (−1.0919) was the most significant in slowing down the LST increase [9]. LCZ D (0.4285) had a positive contribution to the thermal environment of the study area, which is dominated by artificial turf. LCZ E (0.0253) and LCZ F (0.0949) made contributions to the LST increase comparable to LCZ 6 and LCZ 9.

3.5. Optimal LCZ Combinations and Configurations

Blue-green space is known to have a cooling effect [67]. The combination and configuration of LCZs also directly affect the high and low LST [68]. Matching LCZ types to achieve better cooling with less blue-green space in the urban core is defined as the optimal LCZ combination and configuration [69]. In order to explore the optimal LCZ combinations and configurations, 159 blocks in the core area of Fuzhou were selected as the data source, and the area percentages of LCZ types present in each block and the average temperature of the block were statistically derived. The LCZ combinations and configurations among the blocks differed greatly and were statistically combined and categorized into 12 pairings, each corresponding to a temperature range of 31~42 °C (Figure 6).

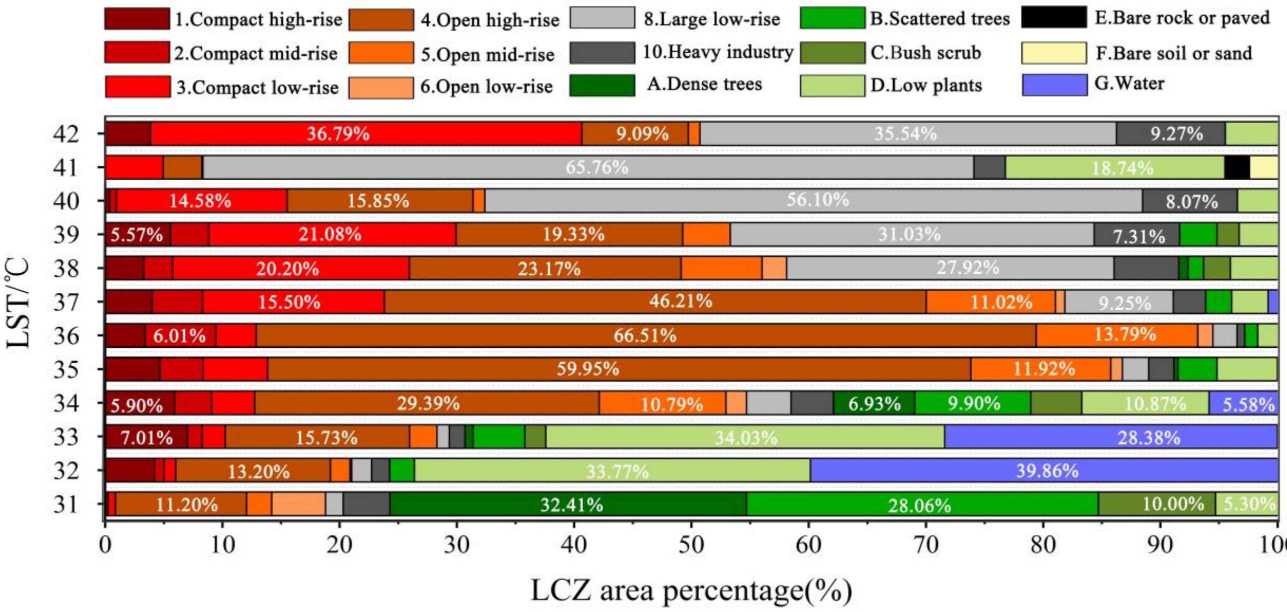

Figure 6. The proportion of LCZ type area to street area in different temperature ranges.

As the results in Figure 7 show, the block with an average LST of 36 °C had the most cost-effective cooling, and the combination and configuration of LCZs within such blocks were the best. From Figure 7a,b, it can be seen that the percentage of green space (LCZ A, LCZ B, and LCZ C) was extremely large when the LST was 34 °C, and the percentage of both green space and blue space (LCZ G) tended to flatten out in the temperature band from 35 to 41 °C. As can be seen from Figure 7c, LCZ 2, LCZ 4, and LCZ 5 were the main building types in the urban core, and their share was the maximum at an LST of 36 °C, while the share of LCZ 10 and LCZ D was the minimum at an LST of 36 °C, which illustrates that the zones with an average LST of 36 °C had the largest share of building types and less area for blue-green space. When the average LST of the block was less than 34 °C, the share of LCZ G spiked (Figure 7b), while the shares of LCZ 2, LCZ 4, and LCZ 5 decreased (Figure 7c), and it is clearly not cost-effective to make the block smaller to lower this temperature. When the average LST of the block was 34~36 °C, the percentages of LCZ A, LCZ B, LCZ C, and LCZ G gradually increased with the decrease in temperature, accompanied by the decrease in LCZ 2, LCZ 4, and LCZ 5. This indicates that, to reduce the temperature of the block within this temperature range, it is necessary to reduce the corresponding building area while increasing the area of blue-green space; the average LST of the block in this temperature range was the highest, mainly along the Jin'an and Min Rivers (Figure 7d). In summary, it can be seen that blocks with an average LST of 36 °C had the most cost-effective cooling, and the combination and configuration of LCZs within such blocks were optimal.

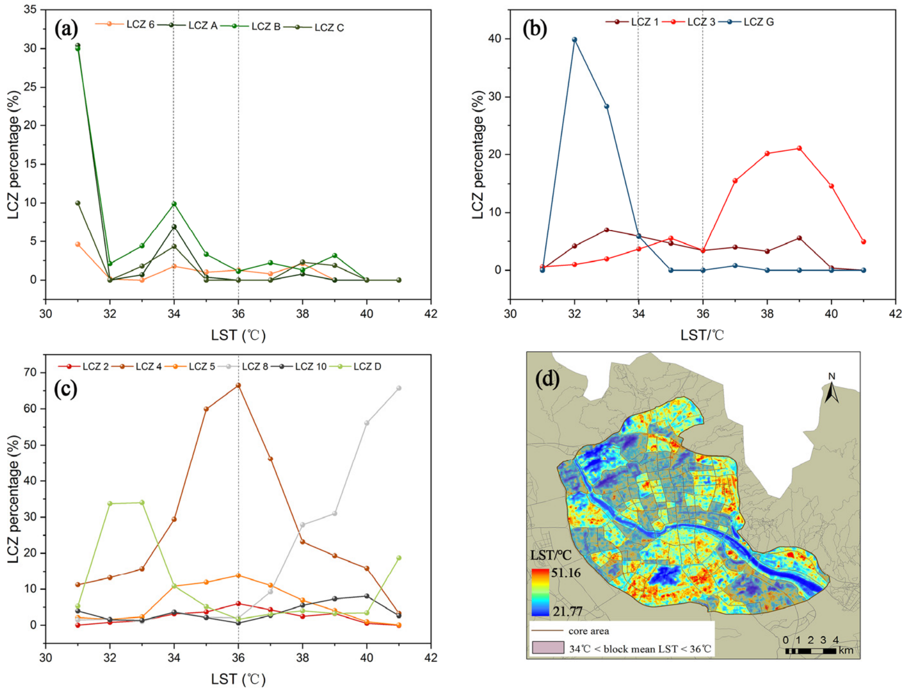

Figure 7. Relationship between the percentage of area of each LCZ type in the blocks of the core zone and the average LST of the blocks: (**a**–**d**) distribution of blocks with an average LST of 34~36 °C.

4. Discussion

4.1. Analysis of the Impact of LCZ Types on the Urban Thermal Environment

The results of the study indicated that the lower temperature zones were mainly located outside the core zone and were dominated by a large number of LCZs (A–C) and LCZ G, while the high-temperature zones were mainly clustered in the core zone of Fuzhou, an area occupied by a large number of LCZ building types (Figures 2 and 3). There were differences in LST across LCZs, with the highest mean LST in low-rise buildings (LCZ 3 (41.67 °C), LCZ 7 (40.10 °C), LCZ 8 (42.61 °C), and LCZ 10 (41.85 °C)), and the lowest mean LST in LCZ A (31.62 °C), and LCZ G (30.58 °C), which is in line with previous studies [22,34,69]. By calculating the thermal contribution of LCZs, the results showed that low and denser LCZs (3, 8, 10) were the main contributors to the rise in LST, while LCZ A, LCZ B, LCZ C, and LCZ G were the main land classes that slowed down the LST rise.

Figure 8a–c shows the hottest blocks in the entire study area, with an average LST of 39–42 °C. LCZ 3 and LCZ 8 in these blocks comprised more than 60% of the block area, while LCZ A, LCZ B, and LCZ C comprised less than 20% of the surroundings. Taking the core zone in 2021 as an example, the block shown in Figure 8a is located at Fuzhou Station, which had the highest average LST (41.2 °C), and LCZ 8 is located in the middle of the block, surrounded by compact low and medium-rise buildings and lacking vegetation. The block shown in Figure 8b is located in the Fuzhou Strait International Convention and Exhibition Center, with LCZ 8 at 65.76% and an average LST of 40.31 °C. The cluster of blocks south of Gaogai Mountain, represented by the block shown in Figure 8c, had higher temperatures and was dominated by the patchy aggregations of LCZ 3. Studies in other cities have also found that LCZ 3 and LCZ 8 can cause similar localized high temperatures due to poor airflow in suburban areas [21,70,71]. In addition, the scarcity of trees and the lack of continuous greening and shading can further limit the cooling effect. This suggests that the high-temperature blocks in the study area suffered from an aggregation and large proportion of high LST land types (LCZ 3 and LCZ 8) and a small proportion of low LST land types (LCZ A, LCZ B, and LCZ C). This type of block can be occupied by compact low- to medium-rise buildings around LCZ 8. This increases the building height while increasing the area of green space, constructing "ventilation corridors" to increase space circulation and shaded areas to reduce the temperature of the block [27,37].

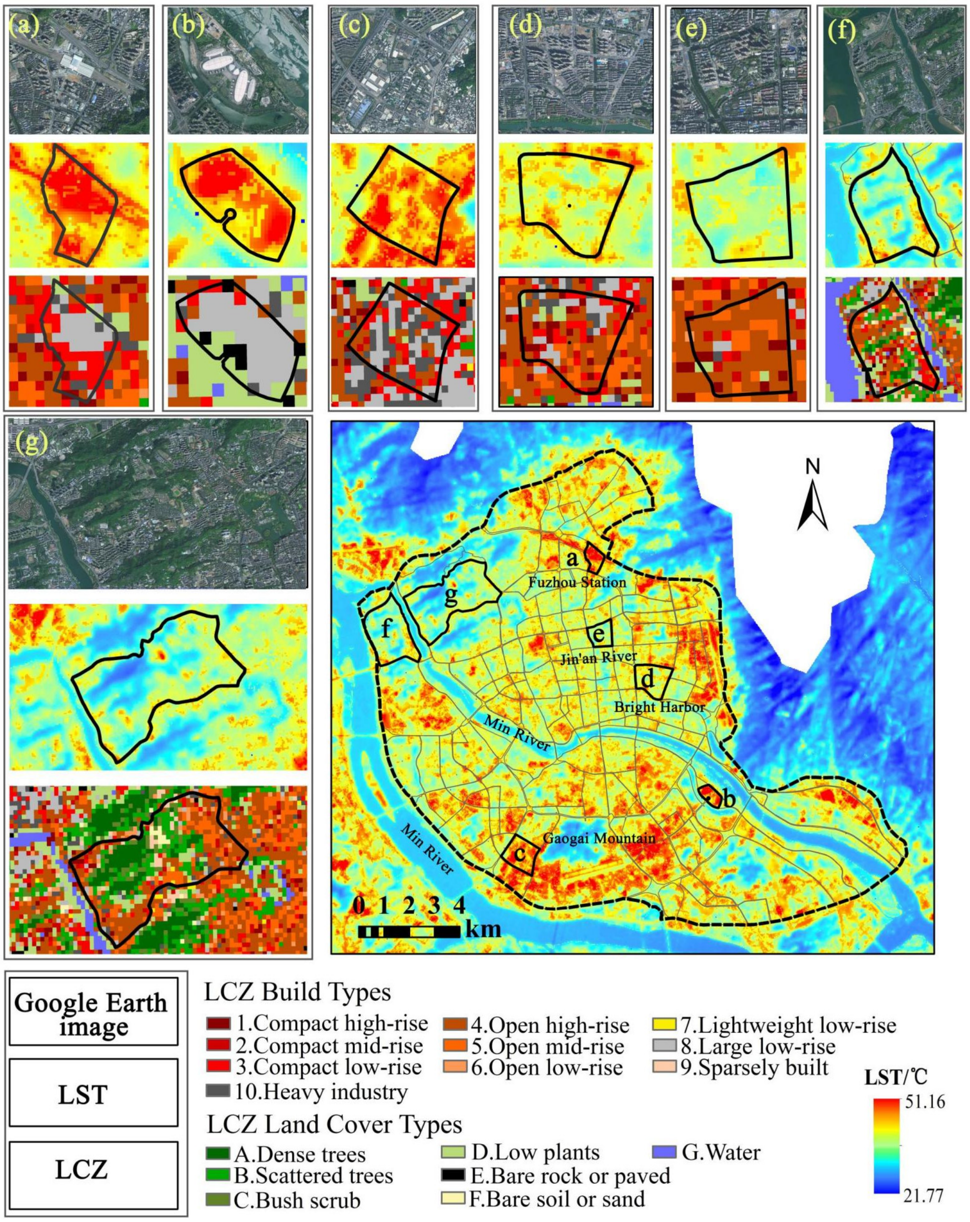

Figure 8. Distribution of the LCZ and LST in different typical areas, (**a**–**g**) represent blocks with different temperature ranges (LST: **a**, **b**, **c** > **d** > **e**, **f** > **g**).

The mean LST was lower in high-rise buildings (LCZ 1 (38.58 °C) and LCZ 4 (38.50 °C)) compared to low and denser LCZs (3, 8, 10). As shown in Figure 8d, the average LST of this type of block was 36–39 °C, with LCZ 4 as the main type, accounting for about 35% of the total, and LCZ 3 and LCZ 8 as the secondary building types. In this temperature range, the LST gradually increased as the proportion of LCZ 4 decreased, which is mainly because building shading reduces solar radiation exposure and plays an important role in lowering urban temperatures [72]. In addition, the efficient airflow and air circulation can also reduce the temperature to a great extent [66,73]. Therefore, blocks in this temperature band can effectively increase airflow and air circulation by increasing the building heights and decreasing the building densities as a means of reducing surface temperatures.

The blocks with an average LST of 34–36 °C can be separated into two categories: the first is the cooling cost-effective type and the second is the type with a balanced share.

The block shown in Figure 8e has a cost-effective type of cooling, with 80% LCZ building types in the block, of which LCZ 4 was the dominant building type. However, the block temperatures were also lower due to the smaller proportion of LCZ 3 and the fact that it is mainly located along the Jin'an River and the Min River. Since the conversion of LCZ 3 into LCZ 4 also represents a decrease in building density and an increase in building height within the block, it can be argued that a decrease in LCZ 3 and an increase in LCZ 4 may have a significant effect in mitigating the urban thermal environment. The block shown in Figure 8f is the balanced type, which has an even distribution of LCZs and is mainly located along the Minjiang River. Because the buildings along the bank are also basically open medium- and high-rise buildings, the cold air from the suburbs enters the inner part of the block to a large extent. At the same time, the water bodies and green areas are interspersed with medium- and low-story buildings to avoid an agglomeration of the low-story buildings, and therefore, the temperature of this block is cooler [27,74].

As shown in Figure 8g, such blocks are mainly distributed along the Min River, with an average LST of 31~34 °C and LCZs (A,B,C), LCZ G, and LCZ D accounting for more than 60% of the total, with almost no LCZ 3 and LCZ 8. Although the temperature of this type of block is low, it also uses a lot of blue-green space and is located along the river, and the small proportion of LCZ 3 and LCZ 8 improves the air circulation and lowers the temperature.

4.2. Some Suggestions for Mitigating the Urban Thermal Environment

Different combinations and configurations of blocks, as well as the influence of neighboring blocks, can lead to large differences in the LST, and cooling should not only combine several factors but also address the particular thermal environment of the block.

From the results for the central city of Fuzhou, reducing the temperature of the 34~36 °C block requires reducing the corresponding building area while increasing the area of blue and green space. In the urban core area, where it is not possible to sacrifice a large amount of building area to increase the blue and green space, we should carefully consider whether it is necessary to change the composition of the LCZ block.

Blocks with an average LST of 36–39 °C simply need to reduce the building density and increase building heights to improve the cooling effect.

Blocks with large low-rise buildings (train stations, large halls, stadiums, etc.) usually have high LSTs, so blindly increasing the area of low-rise vegetation will not have a cooling effect but will increase the temperature. Therefore, when it is difficult to reduce the area of large-scale low-rise buildings in such high-temperature areas, the best way to reduce the temperature is to change the low-rise vegetation to forests and water bodies, which are the most effective in reducing the temperature.

4.3. Limitations and Future Research Directions

Due to the standardization and global applicability of LCZ systems, our proposed optimal LCZ combinations and configurations within zones can be used as a reference for urban planning when considering thermal adaptation in neighborhoods, and as a basis for LCZ layout adjustments within high surface temperature zones. The study of optimal LCZ combinations and configurations within the block is important in mitigating urban thermal environments. Nonetheless, there are some limitations to this study. First of all, considering the availability and comparability of remote sensing image data, only one day's remote sensing image data in summer were used for each year to represent the temporal changes, ignoring the seasonal and daily changes; this possibly led to a certain degree of one-sidedness in the research results. Utilizing different methods for obtaining temperature data in subsequent studies, considering seasonal and diurnal variations, and exploring the effects of jet lag from a more comprehensive perspective are important directions. Secondly, the OLS method used in this paper to quantify the cooling/warming effect of LCZ combination types is for comparison with SEM. However, OLS may not be a state-of-the-art mathematical analysis method, and more novel methods such as random forests can be investigated in the future. Finally, this study takes the central city of Fuzhou as the research object to statistically derive the blocks with the best LCZ combinations and configurations; however, the difference in the scope of this study may have led to a different degree of change in the results, which should be further examined and constitutes our future research direction.

5. Conclusions

The deteriorating urban thermal environment is increasingly affecting the overall quality of life of urban residents. Integrating LCZ systems in order to mitigate the UHI has become a hot spot of research nowadays, but there has not been any research on the optimal combination and configuration of cooling LCZs in urban blocks. In this paper, LCZ systems were combined to analyze the spatial and temporal variations in the thermal environment of the central area of Fuzhou, and 159 blocks in the core area were selected to explore the optimal LCZ combinations and configurations. The conclusions are as follows:

(1) From 2013 to 2021, the LCZ types in the study area changed significantly, the building layouts in the study area became more open, and the building heights gradually increased. LCZ A and LCZ D were the main LCZ types in the study area, and they were also the ones with the most reduced area.

(2) The LST was higher for low-rise buildings (LCZ 3, LCZ 7, LCZ 8, and LCZ 10) than for high-rise buildings (LCZ 1 and LCZ 4). LCZ D also had a significant effect on the rise in LST. Among the low-rise building types, the LST for dense building types was higher than the LST for open building types.

(3) The regression coefficients of LCZs (1~10) and LCZs (3, 8, 10) were all positive, and the most significant effect on the rise in the LST was from LCZs (1~10). The regression coefficients of LCZs (6, 9), LCZs (A~C, G), and FVC were all negative; the cooling effect of LCZs (A~C, G) on the LST was most significant in 2013 and 2021, and the cooling effect of LCZs (6, 9) on the LST was most significant in 2016.

(4) LCZs (3, 8, 10) were the main contributors to the elevated LST. Among the low building types, the thermal contribution of dense building types was significantly higher than that of open building types. LCZ A, LCZ B, LCZ C, and LCZ G were the primary land classes that slowed a rise in LST.

(5) Blocks with an average LST of 36 °C had the highest cost/performance ratio for cooling, and LCZ combinations and configurations within such blocks were optimal. The blocks with an average LST in the range of 34~36 °C were the most numerous and were mainly located along the Jin'an and Min Rivers.

Urbanization and global warming are unstoppable megatrends now and will continue into the future, and urban heat adaptation can be enhanced through careful urban planning strategies. The results of this study can guide urban planners in making finer adjustments to the block layout to adapt to extremely hot weather, reduce the serious impact of the heat island effect on urban residents, and greatly improve their living comfort, which will significantly promote sustainable urban development.

Supplementary Materials: The following supporting information can be downloaded at: https://www.mdpi.com/article/10.3390/su16062367/s1, Table S1. Confusion matrix of LCZ classification maps for Fuzhou central urban area, 2013. Table S2. Confusion matrix of LCZ classification maps for Fuzhou central urban area, 2016. Table S3. Confusion matrix of LCZ classification maps for Fuzhou central urban area, 2021. Table S4. Comparison of the temperature of sample points in the study area with the inversion temperature (unit: °C).

Author Contributions: Conceptualization, Y.C. (Yuanbin Cai) and C.G.; methodology, Y.C. (Yuanbin Cai), C.G. and W.P.; validation, Y.C. (Yuanbin Cai), C.G., Y.C. (Yanhong Chen) and W.P.; investigation, Y.C. (Yuanbin Cai) and C.G.; resources, Y.C. (Yuanbin Cai), C.G. and W.P.; data curation, Y.C. (Yuanbin Cai), C.G. and Y.C. (Yanhong Chen); writing—original draft preparation, Y.C. (Yuanbin Cai), C.G., W.P., Y.C. (Yanhong Chen) and Z.W. All authors were involved in improving the quality of this manuscript. All authors have read and agreed to the published version of the manuscript.

Funding: This research was funded by Education Scientific Research Project of Fujian Province Education Department, grant number JAT200936.

Institutional Review Board Statement: Not applicable.

Informed Consent Statement: Not applicable.

Data Availability Statement: The data presented in this study are available on request from the corresponding author.

Acknowledgments: We are sincerely grateful to Chinese Academy of Sciences for Landsat image and data processing, to World Urban Database and Access Portal Tools for reference data. We greatly appreciate numerous volunteers for field survey. Furthermore, we feel indebted to anonymous reviewers for their valuable comments and suggestions on adequately advancing the quality of this manuscript.

Conflicts of Interest: The authors declare no conflicts of interest.

References

1. Lin, H.; Ma, W.; Liu, Q. *Ambient Temperature and Health in China*; Springer: Singapore, 2019.
2. Francisco, E.; Pierre, P. Disentangling the trend in the warming of urban areas into global and local factors. *Ann. N. Y. Acad. Sci.* **2021**, *1504*, 230–246. [CrossRef]
3. Peng, J.; Liu, Q.; Xu, Z.; Lyu, D.; Du, Y.; Qiao, R.; Wu, J. How to effectively mitigate urban heat island effect? A perspective of waterbody patch size threshold. *Landsc. Urban Plan.* **2020**, *202*, 103873–103882. [CrossRef]
4. Shanshan, C.; Huazhong, R.; Xin, Y.; Jiaji, D.; Yitong, Z. Geometry and adjacency effects in urban land surface temperature retrieval from high-spatial-resolution thermal infrared images. *Remote Sens. Environ.* **2021**, *262*, 112518–112535. [CrossRef]
5. Oke, T.R. The energetic basis of the urban heat island. *Q. J. R. Meteorol. Soc.* **1982**, *108*, 1–24. [CrossRef]
6. Gabriele, M.; Simone, F.; Markus, S.; Kailiang, Y.; Crowther, T.W.; Naika, M.; Paolo, B.; Katul, G.G.; Elie, B.-Z. Magnitude of urban heat islands largely explained by climate and population. *Nature* **2019**, *573*, 55–60. [CrossRef]
7. Fan, H.; Yu, Z.; Yang, G.; Liu, T.Y.; Liu, T.Y.; Hung, C.H.; Vejre, H. How to cool hot-humid (Asian) cities with urban trees? An optimal landscape size perspective. *Agric. For. Meteorol.* **2019**, *265*, 338–348. [CrossRef]
8. Santarnouris, M.; Kolokotsa, D. On the impact of urban overheating and extreme climatic conditions on housing, energy, comfort and environmental quality of vulnerable population in Europe. *Energy Build.* **2015**, *98*, 125–133. [CrossRef]
9. Yu, Z.; Guo, X.; Jorgensen, G.; Vejre, H. How can urban green spaces be planned for climate adaptation in subtropical cities? *Ecol. Indic.* **2017**, *82*, 152–162. [CrossRef]
10. Yang, G.; Yu, Z.; Jorgensen, G.; Vejre, H. How can urban blue-green space be planned for climate adaption in high-latitude cities? A seasonal perspective. *Sustain. Cities Soc.* **2020**, *53*, 101932–101942. [CrossRef]
11. Weng, Q.H.; Lu, D.S.; Schubring, J. Estimation of land surface temperature-vegetation abundance relationship for urban heat island studies. *Remote Sens. Environ.* **2004**, *89*, 467–483. [CrossRef]
12. Yuan, F.; Bauer, M.E. Comparison of impervious surface area and normalized difference vegetation index as indicators of surface urban heat island effects in Landsat imagery. *Remote Sens. Environ.* **2007**, *106*, 375–386. [CrossRef]
13. Li, X.; Zhou, W.; Ouyang, Z.; Xu, W.; Zheng, H. Spatial pattern of greenspace affects land surface temperature: Evidence from the heavily urbanized Beijing metropolitan area, China. *Landsc. Ecol.* **2012**, *27*, 887–898. [CrossRef]
14. Myint, S.W.; Wentz, E.A.; Brazel, A.J.; Quattrochi, D.A. The impact of distinct anthropogenic and vegetation features on urban warming. *Landsc. Ecol.* **2013**, *28*, 959–978. [CrossRef]
15. Essa, W.; van der Kwast, J.; Verbeiren, B.; Batelaan, O. Downscaling of thermal images over urban areas using the land surface temperature-impervious percentage relationship. *Int. J. Appl. Earth Obs. Geoinf.* **2013**, *23*, 95–108. [CrossRef]
16. Zhang, X.; Zhong, T.; Feng, X.; Wang, K. Estimation of the relationship between vegetation patches and urban land surface temperature with remote sensing. *Int. J. Remote Sens.* **2009**, *30*, 2105–2118. [CrossRef]
17. Li, J.; Song, C.; Cao, L.; Zhu, F.; Meng, X.; Wu, J. Impacts of landscape structure on surface urban heat islands: A case study of Shanghai, China. *Remote Sens. Environ.* **2011**, *115*, 3249–3263. [CrossRef]
18. Rhee, J.; Park, S.; Lu, Z. Relationship between land cover patterns and surface temperature in urban areas. *GIScience Remote Sens.* **2014**, *51*, 521–536. [CrossRef]
19. Das, A.; Saha, P.; Dasgupta, R.; Inacio, M.; Das, M.; Pereira, P. How Do the Dynamics of Urbanization Affect the Thermal Environment? A Case from an Urban Agglomeration in Lower Gangetic Plain (India). *Sustainability* **2024**, *16*, 1147. [CrossRef]
20. Lin, J.; Wei, K.; Guan, Z. Exploring the connection between morphological characteristic of built-up areas and surface heat islands based on MSPA. *Urban Clim.* **2024**, *53*, 101764. [CrossRef]
21. Xiang, Y.; Tang, Y.; Wang, Z.; Peng, C.; Huang, C.; Dian, Y.; Teng, M.; Zhou, Z. Seasonal Variations of the Relationship between Spectral Indexes and Land Surface Temperature Based on Local Climate Zones: A Study in Three Yangtze River Megacities. *Remote Sens.* **2023**, *15*, 870–887. [CrossRef]

22. Chen, Y.; Li, J.; Hu, Y.; Liu, L. Spatial and temporal characteristics of nighttime UHII based on local climate zone scheme using mobile measurement—A case study of Changsha. *Build. Environ.* **2023**, *228*, 109869–109886. [CrossRef]
23. Iping, A.; Kidston-Lattari, J.; Simpson-Young, A.; Duncan, E.; McManus, P. (Re)presenting urban heat islands in Australian cities: A study of media reporting and implications for urban heat and climate change debates. *Urban Clim.* **2019**, *27*, 420–429. [CrossRef]
24. Stewart, I.D.; Oke, T.R. Local Climate Zones for Urban Temperature Studies. *Bull. Am. Meteorol. Soc.* **2012**, *93*, 1879–1900. [CrossRef]
25. Wang, R.; Cai, M.; Ren, C.; Bechtel, B.; Xu, Y.; Ng, E. Detecting multi-temporal land cover change and land surface temperature in Pearl River Delta by adopting local climate zone. *Urban Clim.* **2019**, *28*, 100455. [CrossRef]
26. Stewart, I.D. A systematic review and scientific critique of methodology in modern urban heat island literature. *Int. J. Climatol.* **2011**, *31*, 200–217. [CrossRef]
27. Lin, Z.; Xu, H.; Yao, X.; Yang, C.; Yang, L. Exploring the relationship between thermal environmental factors and land surface temperature of a "furnace city" based on local climate zones. *Build. Environ.* **2023**, *243*, 110732–110745. [CrossRef]
28. Bechtel, B.; Daneke, C. Classification of Local Climate Zones Based on Multiple Earth Observation Data. *IEEE J. Sel. Top. Appl. Earth Obs. Remote Sens.* **2012**, *5*, 1191–1202. [CrossRef]
29. Perera, N.G.R.; Emmanuel, R. A "Local Climate Zone" based approach to urban planning in Colombo, Sri Lanka. *Urban Clim.* **2018**, *23*, 188–203. [CrossRef]
30. Ching, J.; Mills, G.; Bechtel, B.; See, L.; Feddema, J.; Wang, X.; Ren, C.; Brousse, O.; Martilli, A.; Neophytou, M.; et al. WUDAPT: An Urban Weather, Climate, and Environmental Modeling Infrastructure for the Anthropocene. *Bull. Am. Meteorol. Soc.* **2018**, *99*, 1907–1924. [CrossRef]
31. Peiró, M.N.; Sánchez, C.S.-G.; González, F.J.N. Source area definition for local climate zones studies. A systematic review. *Build. Environ.* **2019**, *148*, 258–285. [CrossRef]
32. Yuan, B.; Zhou, L.; Hu, F.; Zhang, Q. Diurnal dynamics of heat exposure in Xi'an: A perspective from local climate zone. *Build. Environ.* **2022**, *222*, 109400. [CrossRef]
33. Wang, Y.; Ni, Z.; Hu, M.; Chen, S.; Xia, B. A practical approach of urban green infrastructure planning to mitigate urban overheating: A case study of Guangzhou. *J. Clean. Prod.* **2021**, *287*, 124995. [CrossRef]
34. Wu, J.; Liu, C.; Wang, H. Analysis of Spatio-temporal patterns and related factors of thermal comfort in subtropical coastal cities based on local climate zones. *Build. Environ.* **2022**, *207*, 108568. [CrossRef]
35. Xu, H.; Hu, X.; Guan, H.; He, G. Development of a fine-scale discomfort index map and its application in measuring living environments using remotely-sensed thermal infrared imagery. *Energy Build.* **2017**, *150*, 598–607. [CrossRef]
36. Cai, Y.-B.; Li, K.; Chen, Y.-H.; Wu, L.; Pan, W.-B. The Changes of Heat Contribution Index in Urban Thermal Environment: A Case Study in Fuzhou. *Sustainability* **2021**, *13*, 9638. [CrossRef]
37. Cai, Y.-B.; Wu, Z.-J.; Chen, Y.-H.; Wu, L.; Pan, W.-B. Investigate the Difference of Cooling Effect between Water Bodies and Green Spaces: The Study of Fuzhou, China. *Water* **2022**, *14*, 1471. [CrossRef]
38. Cai, Y.; Chen, Y.; Tong, C. Spatiotemporal evolution of urban green space and its impact on the urban thermal environment based on remote sensing data: A case study of Fuzhou City, China. *Urban For. Urban Green.* **2019**, *41*, 333–343. [CrossRef]
39. Danylo, O.; See, L.; Bechtel, B.; Schepaschenko, D.; Fritz, S. Contributing to WUDAPT: A Local Climate Zone Classification of Two Cities in Ukraine. *IEEE J. Sel. Top. Appl. Earth Obs. Remote Sens.* **2016**, *9*, 1841–1853. [CrossRef]
40. Verdonck, M.-L.; Okujeni, A.; van der Linden, S.; Demuzere, M.; De Wulf, R.; Van Coillie, F. Influence of neighbourhood information on 'Local Climate Zone' mapping in heterogeneous cities. *Int. J. Appl. Earth Obs. Geoinf.* **2017**, *62*, 102–113. [CrossRef]
41. Cai, M.; Ren, C.; Xu, Y.; Lau, K.; Wang, R. Investigating the relationship between local climate zone and land surface temperature using an improved WUDAPT methodology—A case study of Yangtze River Delta, China. *Urban Clim.* **2018**, *24*, 485–502. [CrossRef]
42. Mitraka, Z.; Frate, F.D.; Chrysoulakis, N.; Gastellu-Etchegorry, J.P. Exploiting Earth Observation data products for mapping Local Climate Zones. In Proceedings of the 2015 Joint Urban Remote Sensing Event (JURSE), Lausanne, Switzerland, 30 March–1 April 2015; pp. 1–4.
43. Zheng, Y.; Ren, C.; Xu, Y.; Wang, R.; Ho, J.; Lau, K.; Ng, E. GIS-based mapping of Local Climate Zone in the high-density city of Hong Kong. *Urban Clim.* **2018**, *24*, 419–448. [CrossRef]
44. Geletič, J.; Lehnert, M.; Dobrovolný, P. Land Surface Temperature Differences within Local Climate Zones, Based on Two Central European Cities. *Remote Sens.* **2016**, *8*, 788–805. [CrossRef]
45. Bande, L.; Manandhar, P.; Marpu, P.; Battah, M.A. Local Climate Zones Definition in Relation to ENVI-met in the City of Dubai, UAE. *IOP Conf. Ser. Mater. Sci. Eng.* **2020**, *829*, 012013. [CrossRef]
46. Estacio, I.; Babaan, J.; Pecson, N.J.; Blanco, A.C.; Escoto, J.E.; Alcantara, C.K. Gis-Based Mapping of Local Climate Zones Using Fuzzy Logic and Cellular Automata. *Int. Arch. Photogramm. Remote Sens. Spat. Inf. Sci.* **2019**, *XLII-4/W19*, 199–206. [CrossRef]
47. Gholami, R.; Beck, C. Towards the determination of driving factors of varying LST-LCZ relationships: A case study over 25 cities. *Geogr. Pannonica* **2019**, *23*, 289–307. [CrossRef]
48. Bechtel, B.; Demuzere, M.; Mills, G.; Zhan, W.; Sismanidis, P.; Small, C.; Voogt, J. SUHI analysis using Local Climate Zones—A comparison of 50 cities. *Urban Clim.* **2019**, *28*, 100451. [CrossRef]
49. Middel, A.; Häb, K.; Brazel, A.J.; Martin, C.A.; Guhathakurta, S. Impact of urban form and design on mid-afternoon microclimate in Phoenix Local Climate Zones. *Landsc. Urban Plan.* **2014**, *122*, 16–28. [CrossRef]

50. Bechtel, B.; Alexander, P.J.; Böhner, J.; Ching, J.; Conrad, O.; Feddema, J.; Mills, G.; See, L.; Stewart, I. Mapping Local Climate Zones for a Worldwide Database of the Form and Function of Cities. *ISPRS Int. J. Geo-Inf.* **2015**, *4*, 199–219. [CrossRef]
51. Gillespie, A.; Rokugawa, S.; Matsunaga, T.; Cothern, J.S.; Hook, S.; Kahle, A.B. A temperature and emissivity separation algorithm for Advanced Spaceborne Thermal Emission and Reflection Radiometer (ASTER) images. *IEEE Trans. Geosci. Remote Sens.* **1998**, *36*, 1113–1126. [CrossRef]
52. Jimenez-Munoz, J.C.; Sobrino, J.A.; Skokovic, D.; Mattar, C.; Cristobal, J. Land Surface Temperature Retrieval Methods From Landsat-8 Thermal Infrared Sensor Data. *IEEE Geosci. Remote Sens. Lett.* **2014**, *11*, 1840–1843. [CrossRef]
53. Rozenstein, O.; Qin, Z.; Derimian, Y.; Karnieli, A. Derivation of Land Surface Temperature for Landsat-8 TIRS Using a Split Window Algorithm. *Sensors* **2014**, *14*, 5768–5780. [CrossRef] [PubMed]
54. Jimenez-Munoz, J.C.; Cristobal, J.; Sobrino, J.A. Revision of the single-channel algorithm for land surface temperature retrieval from landsat thermal-infrared data (Article). *IEEE Trans. Geosci. Remote Sens.* **2009**, *47*, 339–349. [CrossRef]
55. Xu, S. An approach to analyzing the intensity of the daytime surface urban heat island effect at a local scale. *Environ. Monit. Assess.* **2009**, *151*, 289–300. [CrossRef] [PubMed]
56. Tarawally, M.; Xu, W.; Hou, W.; Mushore, T.D. Comparative Analysis of Responses of Land Surface Temperature to Long-Term Land Use/Cover Changes between a Coastal and Inland City: A Case of Freetown and Bo Town in Sierra Leone. *Remote Sens.* **2018**, *10*, 112–129. [CrossRef]
57. Ziaul, S.; Pal, S. Analyzing control of respiratory particulate matter on Land Surface Temperature in local climatic zones of English Bazar Municipality and Surroundings. *Urban Clim.* **2018**, *24*, 34–50. [CrossRef]
58. Gao, Y.; Zhao, J.; Han, L. Exploring the spatial heterogeneity of urban heat island effect and its relationship to block morphology with the geographically weighted regression model. *Sustain. Cities Soc.* **2022**, *76*, 103431. [CrossRef]
59. Sookuk, P.; Josangman; Hyun, C.J.; Kong, H.Y.; Kim, S.H.; Shin, Y.-K. Air Temperature Modification of an Urban Neighborhood Park in Summer—Hyowon Park, Suwon-si, Gyeonggi-do. *J. Environ. Sci. Int.* **2017**, *26*, 1057–1072. [CrossRef]
60. Jia, D.; Kaishan, S.; Baohua, Y. Impact of the Zhalong Wetland on Neighboring Land Surface Temperature Based on Remote Sensing and GIS. *Chin. Geogr. Sci.* **2019**, *29*, 798–808. [CrossRef]
61. Sun, R.; Chen, A.; Chen, L.; Lu, Y. Cooling effects of wetlands in an urban region: The case of Beijing. *Ecol. Indic.* **2012**, *20*, 57–64. [CrossRef]
62. Leconte, F.; Bouyer, J.; Claverie, R.; Petrissans, M. Using Local Climate Zone scheme for UHI assessment: Evaluation of the method using mobile measurements. *Build. Environ.* **2015**, *83*, 39–49. [CrossRef]
63. Yang, X.; Yao, L.; Jin, T.; Peng, L.L.H.; Jiang, Z.; Hu, Z.; Ye, Y. Assessing the thermal behavior of different local climate zones in the Nanjing metropolis, China. *Build. Environ.* **2018**, *137*, 171–184. [CrossRef]
64. Qi, Y.; Li, H.; Pang, Z.; Gao, W.; Liu, C. A Case Study of the Relationship Between Vegetation Coverage and Urban Heat Island in a Coastal City by Applying Digital Twins. *Front. Plant Sci.* **2022**, *13*, 861768. [CrossRef]
65. Olander, L.P.; Galik, C.S.; Kissinger, G.A. Operationalizing REDD+: Scope of reduced emissions from deforestation and forest degradation. *Curr. Opin. Environ. Sustain.* **2012**, *4*, 661–669. [CrossRef]
66. Yang, J.; Jin, S.; Xiao, X.; Jin, C.; Xia, J.; Li, X.; Wang, S. Local climate zone ventilation and urban land surface temperatures: Towards a performance-based and wind-sensitive planning proposal in megacities. *Sustain. Cities Soc.* **2019**, *47*, 101487–101497. [CrossRef]
67. Gunawardena, K.R.; Wells, M.J.; Kershaw, T. Utilising green and bluespace to mitigate urban heat island intensity. *Sci. Total Environ.* **2017**, *584–585*, 1040–1055. [CrossRef]
68. Myint, S.W.; Zheng, B.; Talen, E.; Fan, C.; Kaplan, S.; Middel, A.; Smith, M.; Huang, H.-P.; Brazel, A. Does the spatial arrangement of urban landscape matter? Examples of urban warming and cooling in Phoenix and Las Vegas. *Ecosyst. Health Sustain.* **2015**, *1*, 11878989. [CrossRef]
69. Geng, X.; Yu, Z.; Zhang, D.; Li, C.; Yuan, Y.; Wang, X. The influence of local background climate on the dominant factors and threshold-size of the cooling effect of urban parks. *Sci. Total Environ.* **2022**, *823*, 153806. [CrossRef] [PubMed]
70. Wang, R.; Voogt, J.; Ren, C.; Ng, E. Spatial-temporal variations of surface urban heat island: An application of local climate zone into large Chinese cities. *Build. Environ.* **2022**, *222*, 109378–109399. [CrossRef]
71. Roth, M.; Sanchez, B.; Li, R.; Velasco, E. Spatial and temporal characteristics of near-surface air temperature across local climate zones in a tropical city. *Int. J. Climatol.* **2022**, *42*, 9730–9752. [CrossRef]
72. Yu, K.; Chen, Y.; Wang, D.; Chen, Z.; Gong, A.; Li, J. Study of the Seasonal Effect of Building Shadows on Urban Land Surface Temperatures Based on Remote Sensing Data. *Remote Sens.* **2019**, *11*, 497–520. [CrossRef]
73. Wang, M.; Xu, H. The impact of building height on urban thermal environment in summer: A case study of Chinese megacities. *PLoS ONE* **2021**, *16*, e0247786. [CrossRef] [PubMed]
74. Cai, Y.; Zhang, H.; Zheng, P.; Pan, W. Quantifying the Impact of Land use/Land Cover Changes on the Urban Heat Island: A Case Study of the Natural Wetlands Distribution Area of Fuzhou City, China. *Wetlands* **2016**, *36*, 285–298. [CrossRef]